Electronic supplementary information for

Non-destructive Stripping Electrochemistry Enables Long-Life Zinc Metal Batteries

Ruiting Guo[a,b], Xiong Liu*[b], Kun Ni[c], Fanjie Xia[a], Huazhang Zhang[d], Yu Liu[e], Xinzhe Dai[b], Litong Shi[b], Xuanpeng Wang[a,d], Chunhua Han*[a], Liqiang Mai*[a] and Chaojiang Niu*[b]

[a]State Key Laboratory of Advanced Technology for Materials Synthesis and Processing, Wuhan University of Technology, Wuhan 430070, China
[b]School of Materials Science and Engineering, Zhengzhou University, Zhengzhou 450001, China
[c]CAS Key Laboratory of Materials for Energy Conversion, Department of Materials Science and Engineering, iChEM, University of Science and Technology of China, Anhui 230026, China
[d]Department of Physical Science & Technology, School of Physics and Mechanics, Wuhan University of Technology, Wuhan, 430070, China
[e]State Key Laboratory of Refractories and Metallurgy, Institute of Advanced Materials and Nanotechnology, Wuhan University of Science and Technology, Wuhan 430081, China

*Corresponding authors: Chaojiang Niu (niuchaojiang@zzu.edu.cn), Liqiang Mai (mlq518@whut.edu.cn), Chunhua Han (hch5927@whut.edu.cn), Xiong Liu (liuxiong@zzu.edu.cn).

Methods

Preparation of Zn@$Cu_{0.7}Zn_{0.3}$. A piece of Zn foil (1.6 cm × 5 cm) was initially cleaned with alcohol-moistened dust-free paper and subsequently dried at room temperature. Following this, the cleaned foil was immersed in a 0.1 M $CuSO_4$ aqueous solution for 9 s. Subsequently, the reacted foil was promptly removed and washed successively with ultrapure water and alcohol before being dried.

Preparation of Zn_xMnO_2. The cathode material was synthesized using the method reported in our previous work[1]. First, 1.264 g $KMnO_4$ was dissolved in 75 mL deionized water, followed by the sequential addition of 2.379 g $Zn(NO_3)_2\cdot6H_2O$ and 2 mL 98% H_2SO_4. The resulting solution was stirred for 20 min before being transferred to a 100 mL Teflon-lined stainless steel autoclave. The autoclave was then maintained at 140 °C for 3.5 h. Upon cooling to room temperature, the resulting powder was washed with deionized water and alcohol, and finally dried in a 70 °C oven. The yield from a single synthesis was determined to be about 0.7 g.

Material characterizations. A JEOL JSM-7100F scanning electron microscope (SEM) and Thermo Scientific Phenom Pro + SED were used to obtain the surface morphology and corresponding elemental mappings. Grazing-incidence X-ray diffraction (GI-XRD) patterns were obtained with Malvern Panalitical Empyrean at an incidence angle of 1 degree. HAADF-STEM, SAED patterns, and EDS mappings were obtained from a double corrected Titan G2 60-300 electron microscope. The cross-sectional TEM specimen preparation was conducted on a FEI Helios Nanolab G3 UC FIB (Focused ion beam) operating at 2~30 kV. A standard liftout procedure was used to directly prepare thin-section TEM specimens from original and cycled electrodes. Time-of-flight secondary-ion mass spectrometry (Tof-SIMS) analysis was performed using a LION TOF-SIMS 5.

Electrochemical measurements. The as-prepared Zn_xMnO_2 powder, multi-walled carbon nanotubes (MWCNTs) with dimensions ranging from 10 to 20 nm, and polytetrafluoroethylene binder were mixed and ground together in a mass ratio of 7 : 2 : 1. The resulting mixture was then rolled into self-supporting film and cutted into several electrodes, which were subsequently pressed onto titanium mesh (80 mesh, Φ14 mm) and dried at 60 °C for 12 h. The mass loading of the electrodes was maintained at 5~6 mg cm^{-2}. Following this, CR2032-type coin cells were assembled for electrochemical testing, with glass fiber film (GF/D, Whatman) serving as the separator. 2 M $ZnSO_4$ electrolyte was used for bare Zn and $Zn@Cu_{0.7}Zn_{0.3}$ symmetric cells, while a mixture electrolyte of 2 M $ZnSO_4$ + 0.1 M $CuSO_4$ was used for Cu^{2+}-$Zn@Cu_{0.7}Zn_{0.3}$ symmetric cell. For the 85% depth of discharge test, a mixture electrolyte of 2 M $ZnSO_4$ + 0.5 M $CuSO_4$ was used for Cu^{2+}-$Zn@Cu_{0.7}Zn_{0.3}$ symmetric cell. In all tests, a mixture electrolyte of 2 M $ZnSO_4$ + 0.2 M $MnSO_4$ was used. The long-term cycling performance and rate capability were tested by a multichannel battery testing system (LAND CT2001A, Wuhan, China), with the voltage range for full cells set between 0.8 and 1.9 V. Electrochemical impedance spectroscopy (100 kHz ~ 0.01 Hz) was performed using an electrochemical workstation (CHI 760E, Chenhua, China). Specially, the single-layer pouch cell was constructed using a 30 μm-thick Cu^{2+}-$Zn@Cu_{0.7}Zn_{0.3}$ composite foil as the anode and the mixture (Zn_xMnO_2 : MWCNTs : polytetrafluoroethylene binder = 7 : 2 : 1) loaded on titanium mesh with a mass loading of 6.4 mg cm^{-2} as the cathode. The 0.638 Ah pouch cell was constructed using a 50 μm-thick Cu^{2+}-$Zn@Cu_{0.7}Zn_{0.3}$ composite foil as the anode and the mixture (Zn_xMnO_2 : MWCNTs : polytetrafluoroethylene binder = 8 : 1 : 1) loaded on titanium mesh with a mass loading of 19.5 mg cm^{-2} (two sides) as the cathode.

Theoretical calculations. All DFT simulations were performed by using Vienna ab-initio simulation package (VASP) software[2]. The exchange-correlation interactions were described by generalized gradient approximation (GGA)[3] with Perdew-Burke-Ernzerhof (PBE) functional[4]. The energy cutoff of plane wave basis set was 450 eV. Gaussian type smearing with energy window of 0.1 eV was used for optimizations. The energy convergence tolerance was 0.001 meV. The force tolerance for optimization task was 0.01 eV/Å. All calculations were performed with spin unrestricted. The electronic minimization algorithm was "all band simultaneous update of orbitals" with TIME of 0.2. DFT-D3 method was adopted[5]. K points were sampled as 4×4×1 for Zn (002) surface model, which contains 4 layers of Zn atoms with 9 atoms in each layer. The vacuum slab in OC direction was 20 Å. The adsorption energy was expressed as

$$\Delta E_{ads} = E_{\mathrm{A+B}} - E_A - E_B$$

where E_{A+B} was the total energy of slab A model with B molecule, E_A was the energy of a A slab, and E_B was that for a B molecule. Here, differences in Gibbs free energy (ΔG) for intermediates in hydrogen evolution were defined as:

$$\Delta G = \Delta E + \Delta E_{ZPE} - T\Delta S + \Delta G_U$$

where ΔG was the total energy difference between the slab and respective terminations computed by DFT-PBE. ΔE_{ZPE} and TΔS denoted differences in zero-point energy and entropy between adsorbed states of reaction intermediates and gap phase, respectively. T was the room temperature (298.15 K). $\Delta G_U = -eU$, whereby U was the electrode potential.

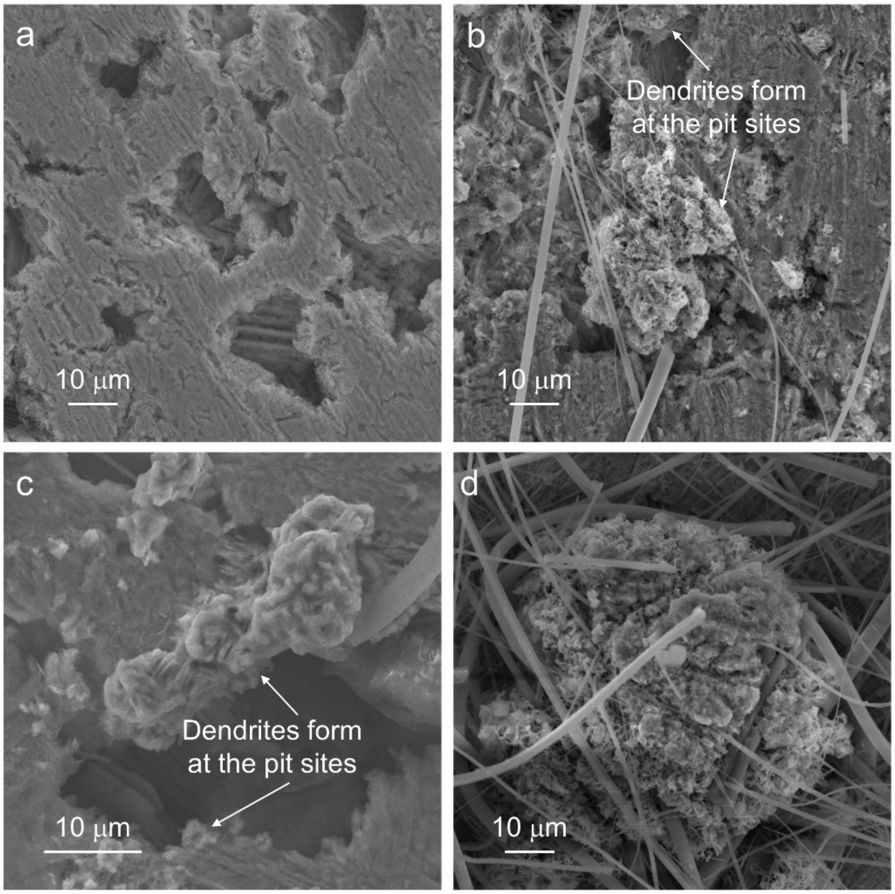

Fig. S1 (a) SEM image of bare Zn surface after stripping for 20 min. (b, c) SEM image of Zn surface after stripping for 60 min and then plating for 20 min. (d) SEM image of Zn surface after stripping for 60 min and then plating for 60 min. The applied current density is 1 mA cm^{-2}.

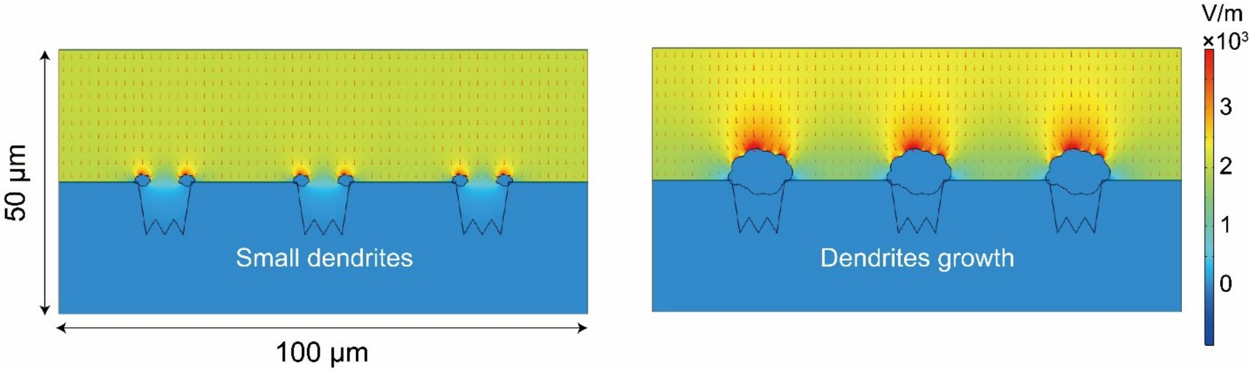

Fig. S2 Simulated electric field distribution of bare Zn surface with pits generated by Zn stripping, where Zn tends to plate and grows into dendrites.

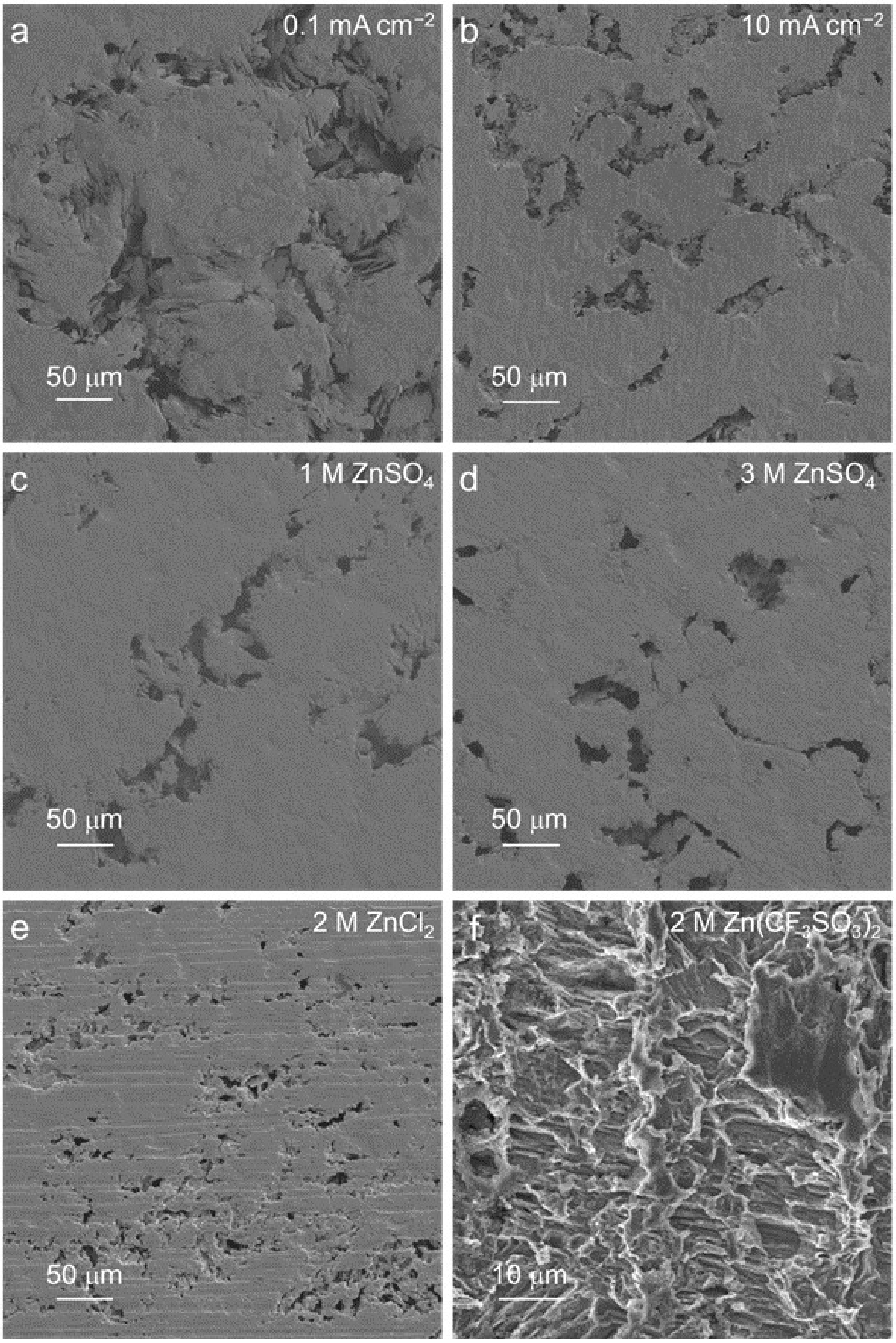

Fig. S3 SEM images of Zn surface after stripping in 2 M $ZnSO_4$ electrolyte at (a) 0.1 and (b) 10 mA cm^{-2} for 1 mAh cm^{-2}. SEM images of Zn surface after stripping in (c) 1 M and (d) 3 M $ZnSO_4$ electrolytes at 1 mA cm^{-2} for 1 mAh cm^{-2}. SEM images of Zn surface after stripping in (e) 2 M $ZnCl_2$ and (f) 2 M $Zn(CF_3SO_3)_2$ electrolytes at 1 mA cm^{-2} for 1 mAh cm^{-2}.

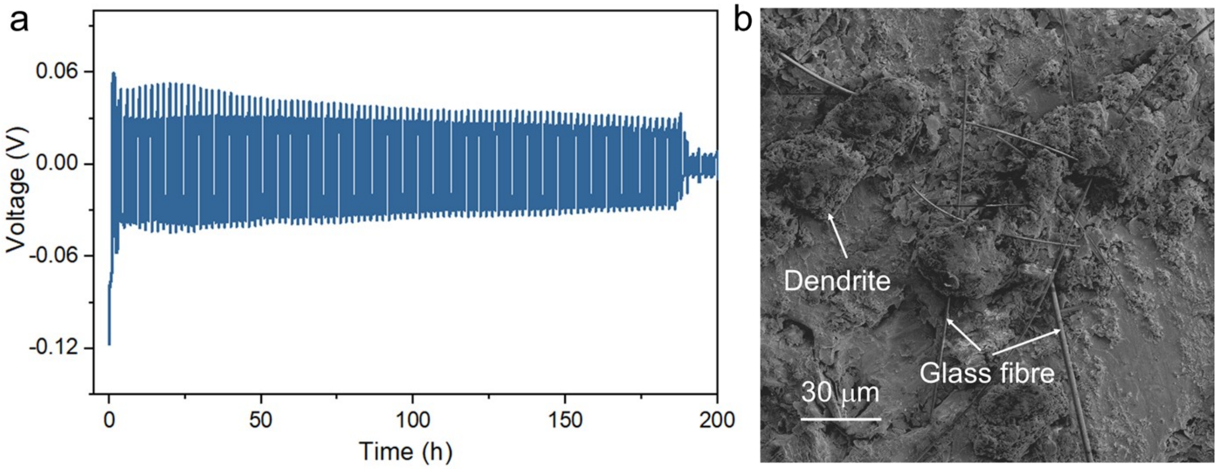

Fig. S4 (a) Symmetric cell of bare Zn under 1 mA cm^{-2} with an areal capacity of 1 mAh cm^{-2}**.** (b) SEM image of bare Zn after 35 cycles in symmetric cell using Zn(CF$_3$SO$_3$)$_2$ electrolyte.

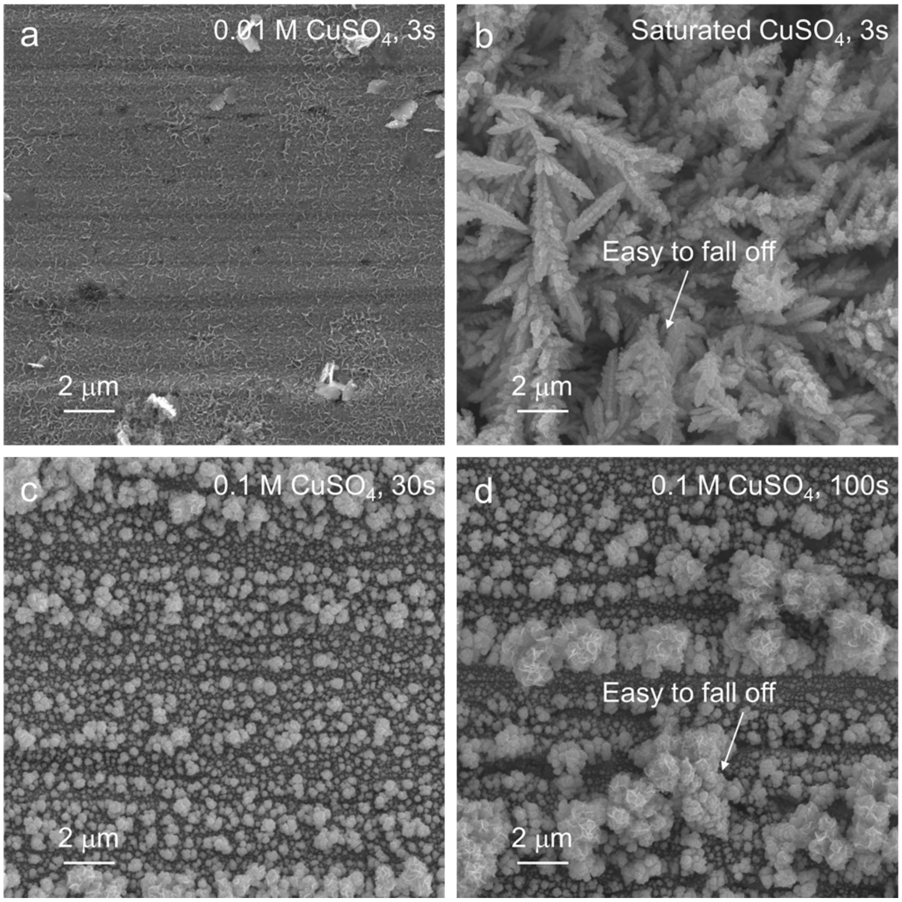

Fig. S5 SEM images of Zn surface after reacting in (a) 0.01 M $CuSO_4$ for 3 s, (b) saturated $CuSO_4$ for 3 s, (c) 0.1 M $CuSO_4$ for 30 s, and (d) 0.1 M $CuSO_4$ for 100 s.

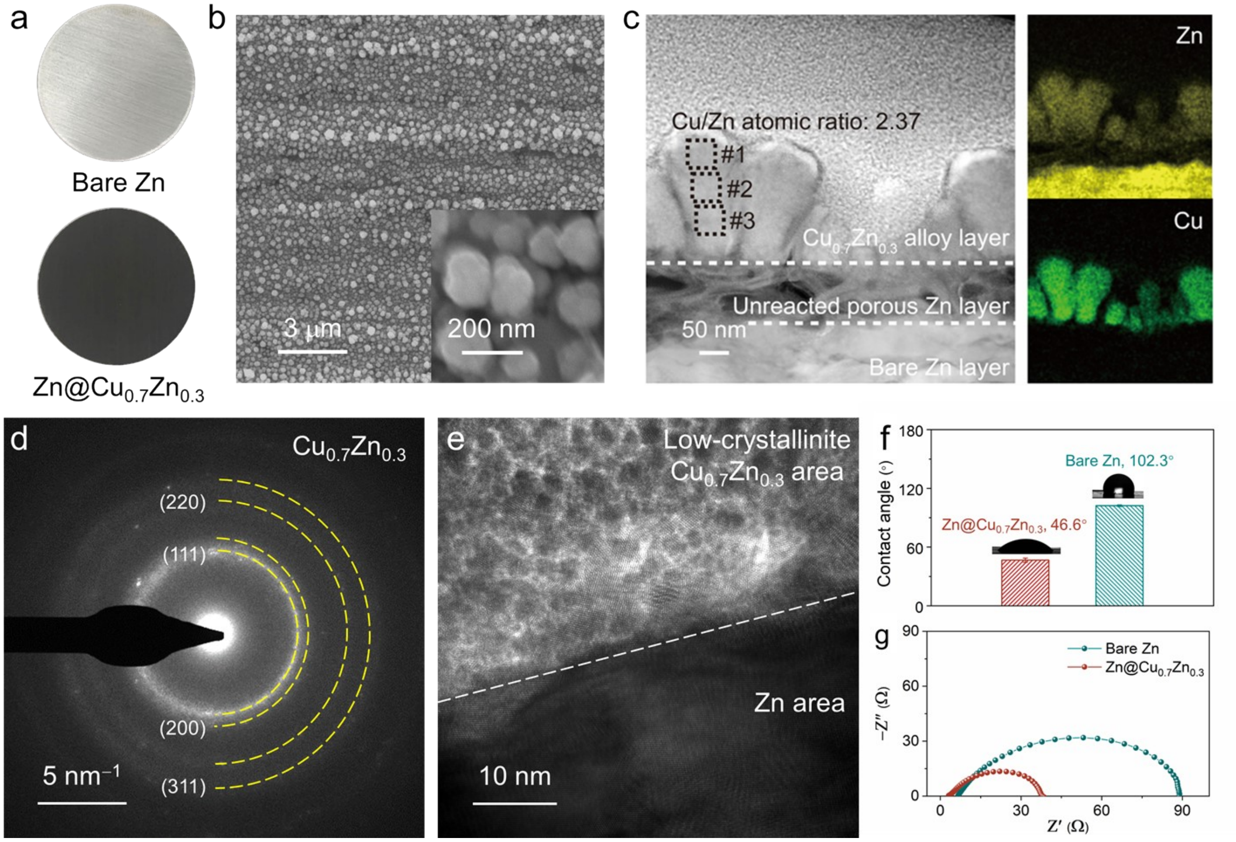

Fig. S6 (a) Optical photographs of bare Zn and Zn@Cu$_{0.7}$Zn$_{0.3}$ foils. (b) SEM image of Zn@Cu$_{0.7}$Zn$_{0.3}$ surface. (c) FIB-STEM image and corresponding mappings of Zn@Cu$_{0.7}$Zn$_{0.3}$ thin section. (d) SAED pattern for Cu$_{0.7}$Zn$_{0.3}$ nanoparticle area, and the diffraction rings in the pattern are well-indexed as (111), (200), (220), and (311) crystal planes of Cu$_{0.7}$Zn$_{0.3}$ (JCPDS No. 03-065-9062). (e) HRTEM image of the interface between Zn and Cu$_{0.7}$Zn$_{0.3}$ areas. (f) Contact angles of 2 M ZnSO$_4$ on bare zinc and Cu$_{0.7}$Zn$_{0.3}$ composite foils. (g) Nyquist plots of bare Zn and Zn@Cu$_{0.7}$Zn$_{0.3}$ symmetric cells.

Table S1 Cu/Zn atomic ratios in multiple areas of particle derived from data in Fig. S6c.

Areas	**Cu**		**Zn**	
	Atomic fraction (%)	Atomic error (%)	Atomic fraction (%)	Atomic error (%)
#1	67.95	6.16	32.05	5.06
#2	69.60	6.12	30.40	4.75
#3	73.49	6.02	26.51	4.06
Average values	70.35	-	29.65	-

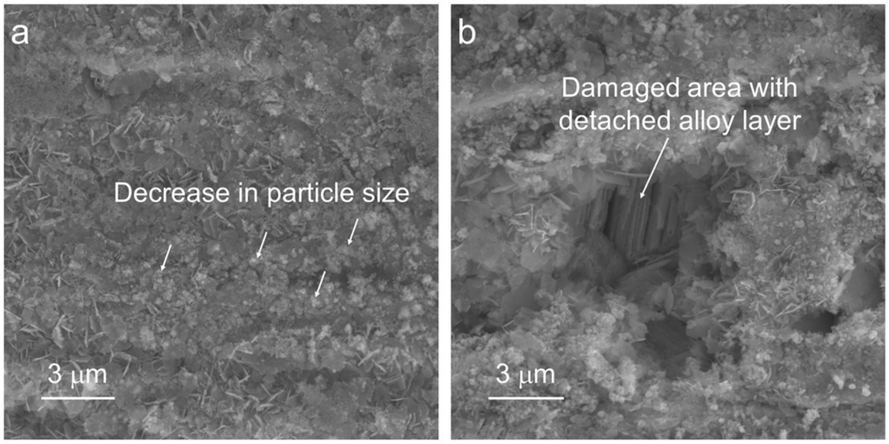

Fig. S7 SEM images of $Zn@Cu_{0.7}Zn_{0.3}$ surface after Zn stripping for (a) 20 min and (b) 40 min.

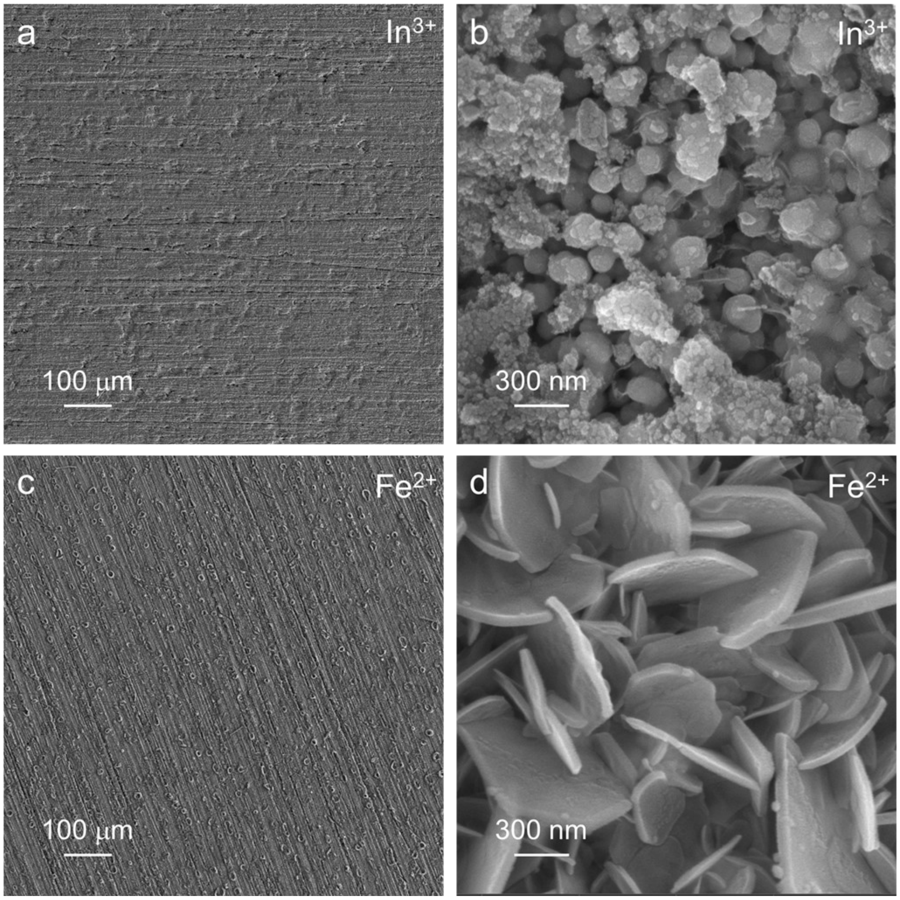

Fig. S8 SEM images of Zn@$Cu_{0.7}Zn_{0.3}$ surface after stripping in (a, b) 2 M $ZnSO_4$ with 5% In^{3+} and (c, d) 2 M $ZnSO_4$ with 5% Fe^{2+} electrolytes tested at 1 mA cm^{-2} for 60 min.

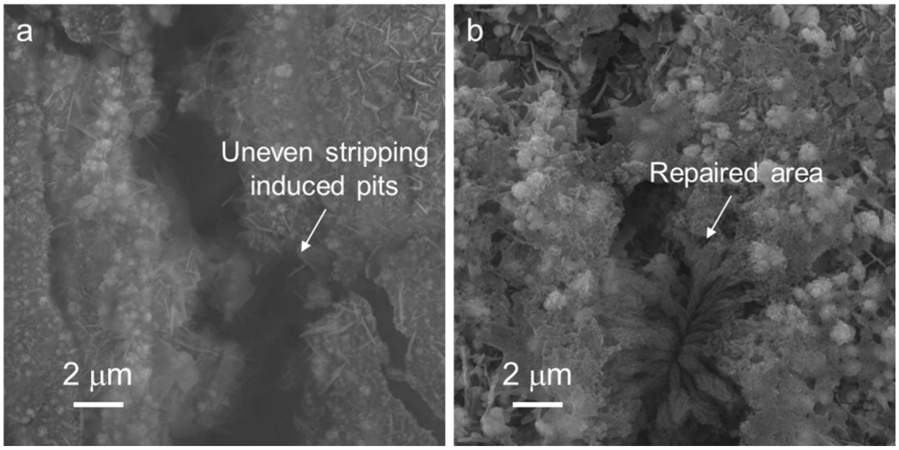

Fig. S9 Identical-location SEM images of Zn@$Cu_{0.7}Zn_{0.3}$ electrode (a) before and (b) after repair.

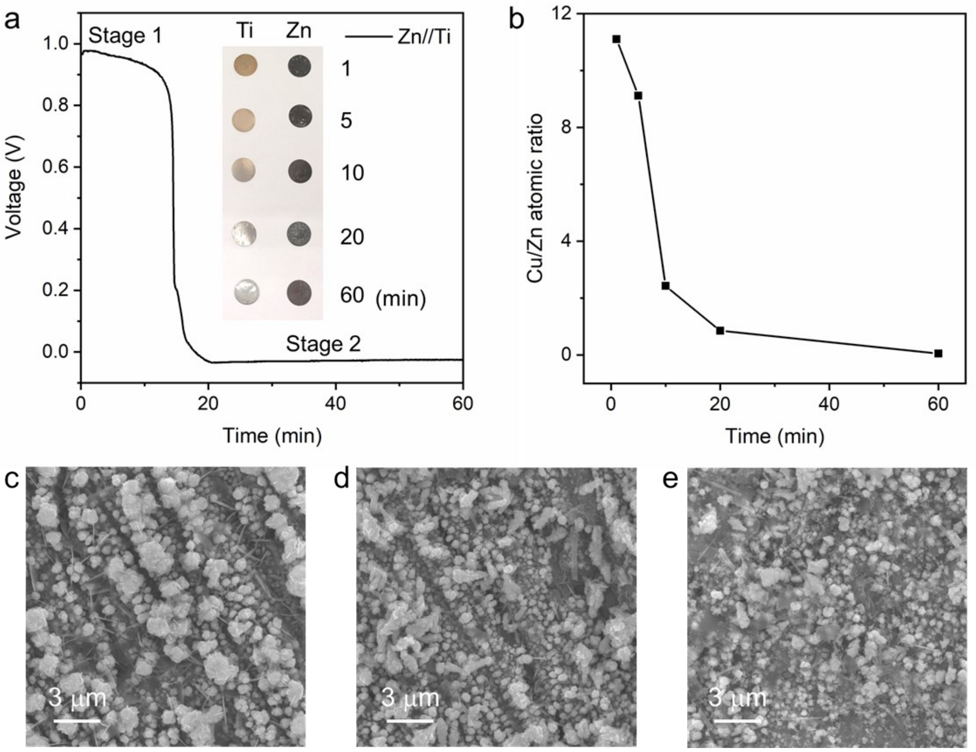

Fig. S10 (a) Discharge curve of Zn//Ti cell at 1 mA cm^{-2}. Insert is the optical photograph of Ti cathode and Zn anode electrodes under different discharge times. (b) Cu/Zn atomic ratios during discharge process determined by X-ray photoelectron spectroscopy (XPS) element analysis. (c-e) SEM images of Zn anodes after discharging for 1, 10, and 60 min.

Note. Zn//Ti asymmetric cell is used to reveal the reason for the increase of polarization voltage from 0 V induced by Cu^{2+}. As shown in **Fig. S10a**, the voltage curve exhibits two platforms at stages 1 and 2. Upon the plating process was performed on Ti foil, the surface initially turns golden within 1 min, gradually lightening until eventually appearing silver. XPS results show that the main component at 1 min is Cu, with the Cu/Zn atomic ratio decreasing rapidly within 20 min (**Fig. S10b**). For Zn anode, its surface changes from silver to black at 1min, accompanied by the appearance of Cu-Zn particles, indicating that a displacement reaction occurs (**Fig. S10c**).

In summary of these results, within symmetric cell, the Zn stripping reaction occurs at the cathode: $Zn - 2e^- = Zn^{2+}$. Spontaneously, Cu^{2+} in the electrolyte undergoes replacement and alloys with freshly exposed Zn, thereby producing more alloy particles and making up for the pits caused by zinc stripping. Simultaneously, due to the higher oxidability of Cu^{2+} compared to Zn^{2+}, Cu^{2+} is preferentially reduced at the anode: $Cu^{2+} + 2e^- = Cu$. This reduction process, characterized by a high potential (0.342 V vs. standard hydrogen electrode), contributes to the initial low cell voltage. Both electrodes consume Cu^{2+}, but Cu^{2+} is trace. Once Cu^{2+} is depleted, the electrode reactions are completely transformed into pure zinc plating and stripping, thereby restoring the voltage to its normal trend.

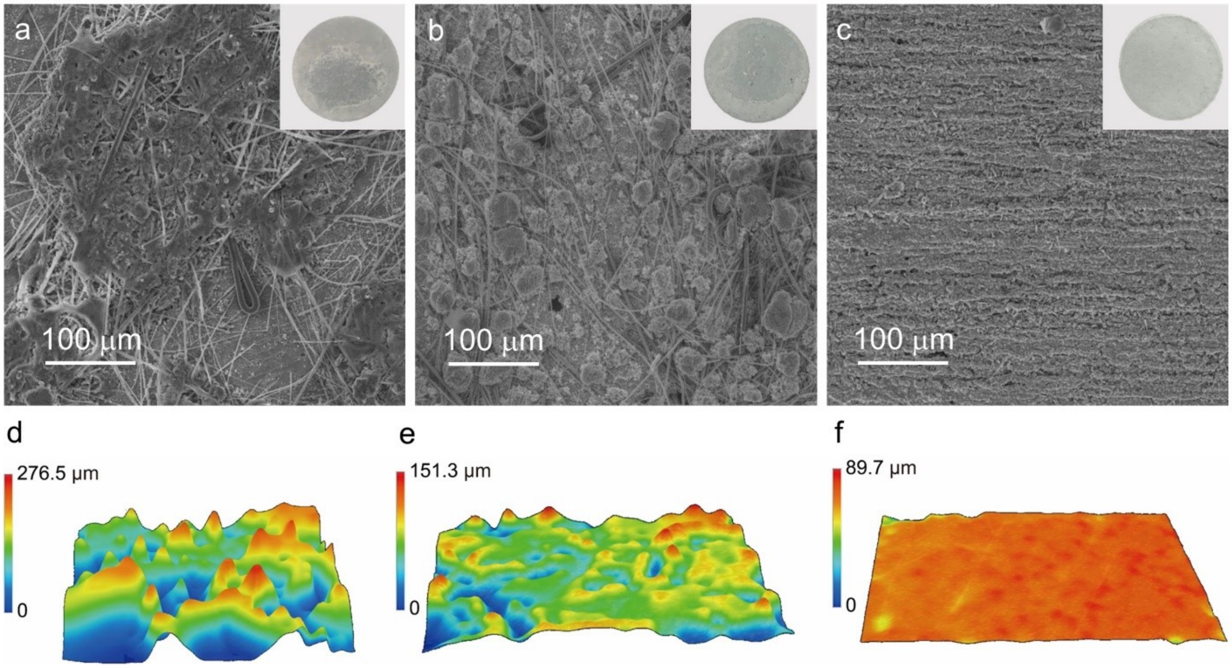

Fig. S11 SEM images and optical photographs of (a) bare Zn, (b) Zn@$Cu_{0.7}Zn_{0.3}$, and (c) Cu^{2+}-Zn@$Cu_{0.7}Zn_{0.3}$ electrodes after cycling at 1 mA cm^{-2} with 1 mAh cm^{-2} per cycle. (d-f) Super depth 3D microscope images of corresponding electrodes after cycling.

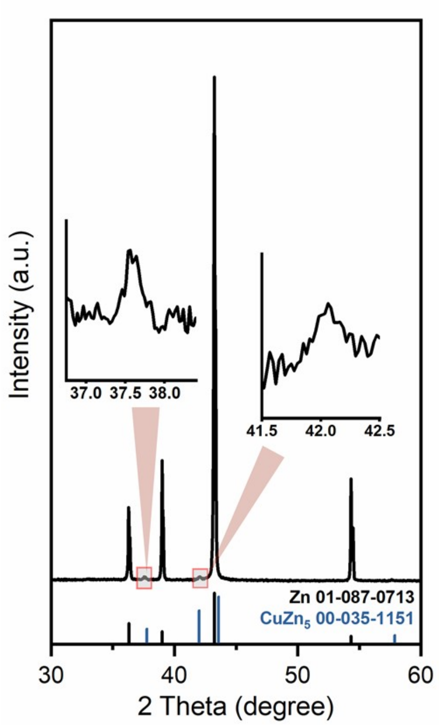

Fig. S12 XRD pattern of Zn@$Cu_{0.7}Zn_{0.3}$ electrode after initial Zn plating.

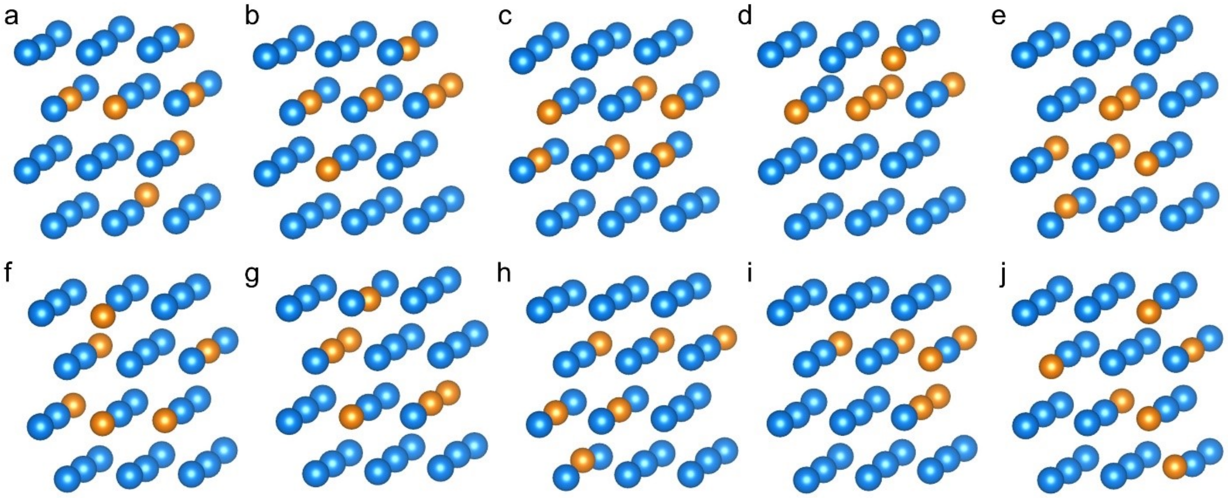

Fig. S13 (a-j) DFT-calculated Cu_6Zn_{30} models (yellow-Cu, blue-Zn) from model-1 to model-10, respectively.

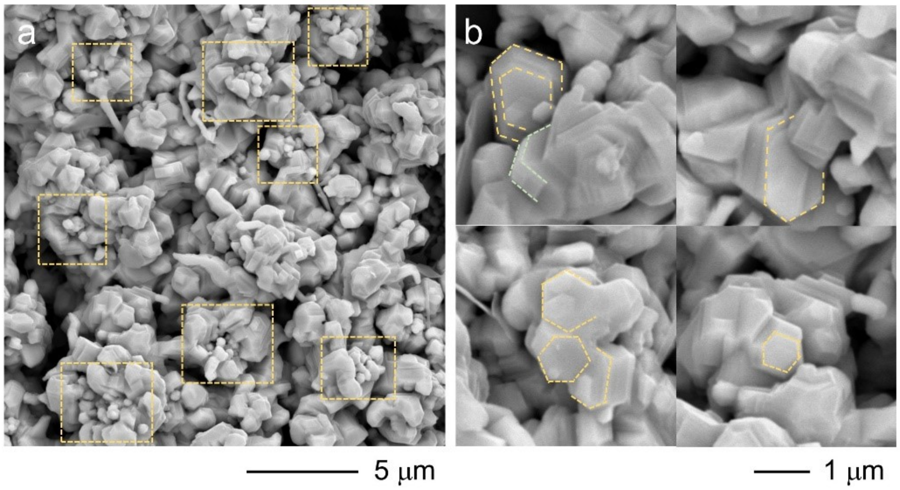

Fig. S14 (a, b) SEM images of Cu^{2+}-Zn@$Cu_{0.7}Zn_{0.3}$ after two cycles.

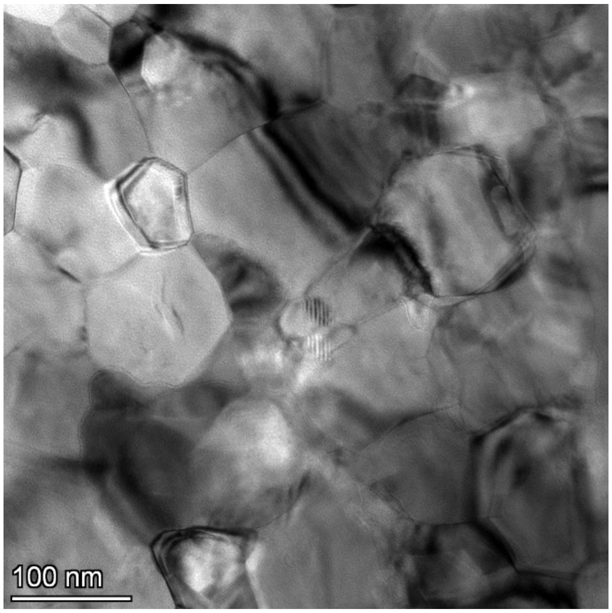

Fig. S15 FIB-TEM image of $CuZn_5$ particles from thin section.

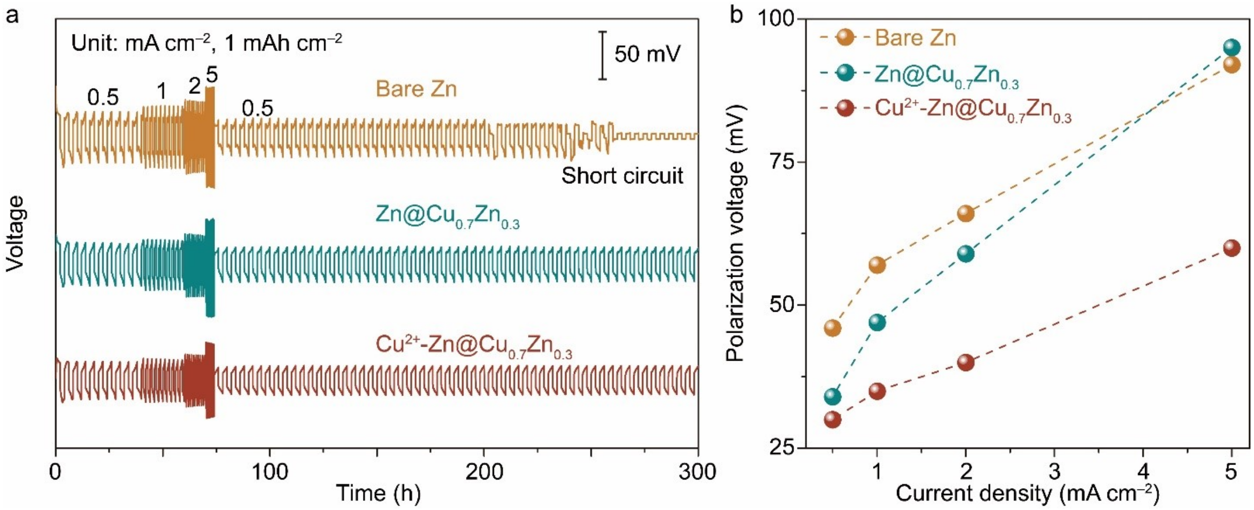

Fig. S16 (a) Rate performance of symmetrical cells with an areal capacity of 1mAh cm^{-2}. (b) The corresponding polarization voltage of three samples.

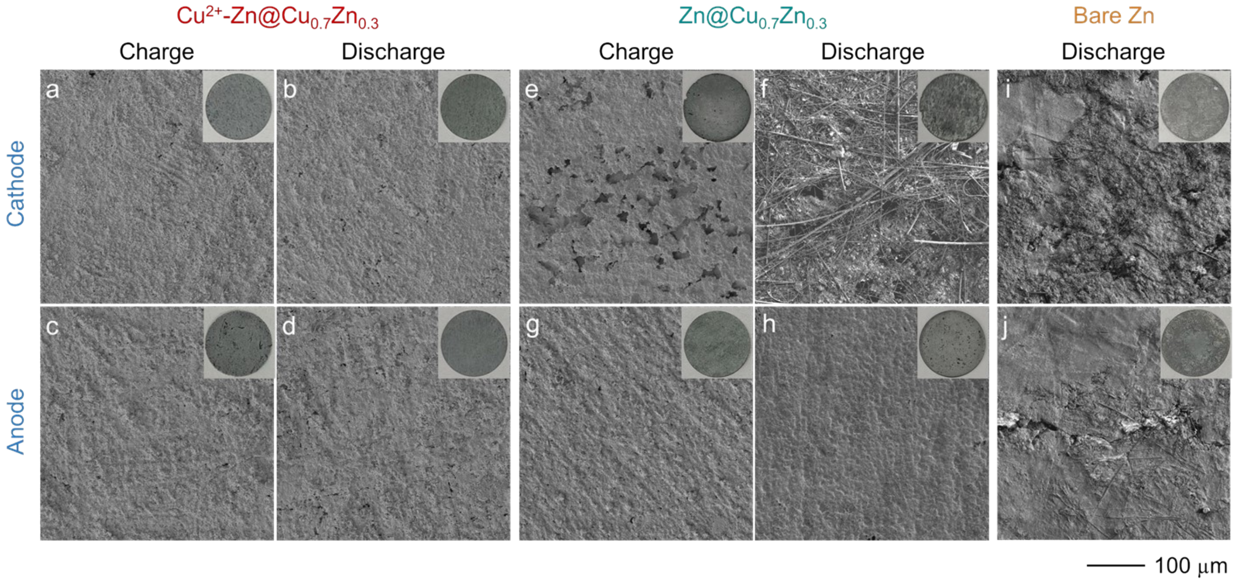

Fig. S17 SEM images and optical photographs (insets) of (a-d) Cu^{2+}-Zn@$Cu_{0.7}Zn_{0.3}$ electrodes, (e-h) Zn@$Cu_{0.7}Zn_{0.3}$ electrodes, and (i, j) bare Zn electrodes.

All symmetric cells perform charge-discharge cycling, that is, Zn stripping-plating cycling occurs at cathode electrode, and the opposite occurs at the anode. For Cu^{2+}-Zn@$Cu_{0.7}Zn_{0.3}$ electrodes, the surfaces of cathode and anode both maintain good integrality, and Zn plating/stripping occurs throughout the electrode surface, showing symmetric states. For Zn@$Cu_{0.7}Zn_{0.3}$ electrodes, the cathode electrode produces pits and dendrites, but the anode maintains well and shows better uniformity, showing asymmetric states. For bare Zn electrodes, pits and dendrites both exist in cathode and anode, showing symmetric states.

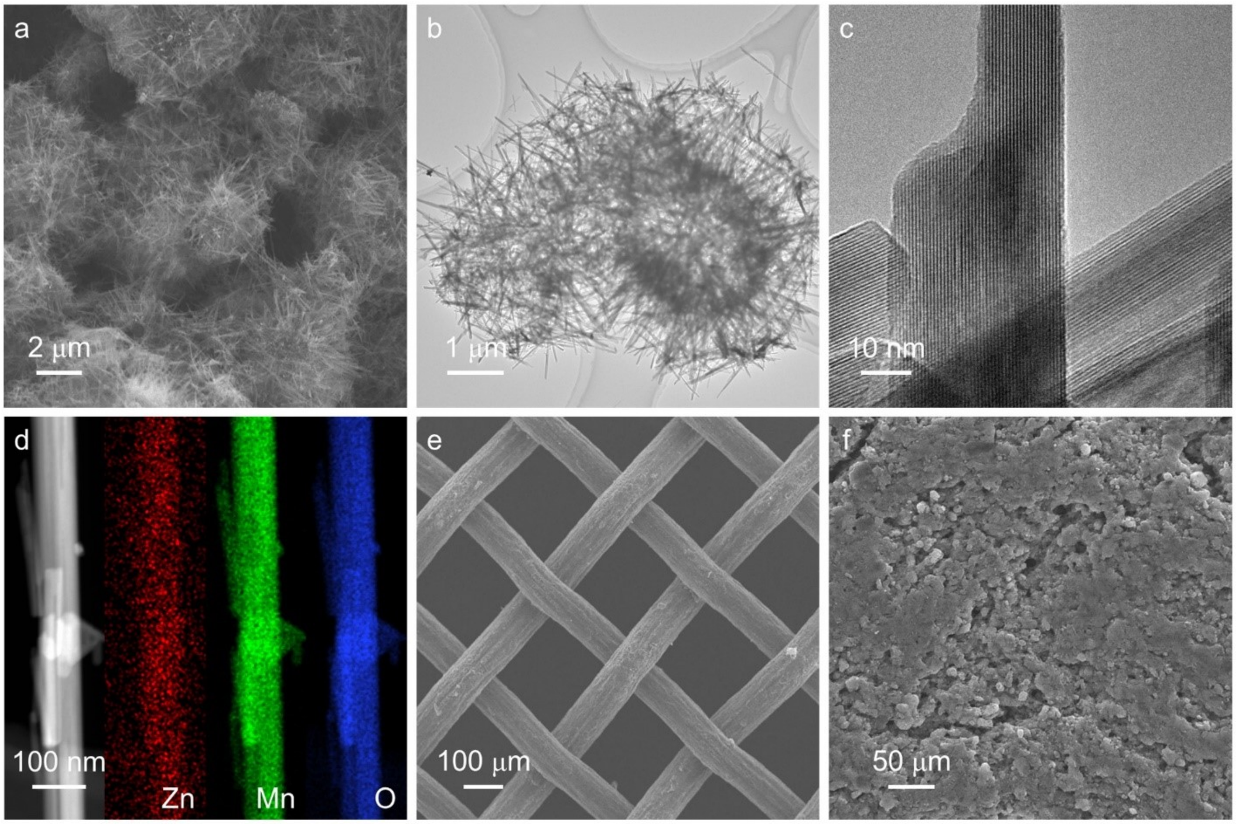

Fig. S18 (a) SEM, (b, c) TEM, and (d) STEM images and corresponding elemental mappings of Zn_xMnO_2 cathode material. (e) SEM image of Ti mesh as a cathode collector. (f) SEM image of Zn_xMnO_2 coated on Ti mesh.

As shown in **Fig. S18a-c**, the Zn_xMnO_2 cathode material exhibits a single-crystal nanowire morphology, with nanowire lengths around 2 μm and diameters ranging from 30 to 50 μm. The element mapping reveals a homogeneous distribution of Zn, Mn, and O elements across the nanowire (**Fig. S18d**).

Table S2 Comparison of the cumulative capacity and cycle number at low current densities obtained in this work to previously reported values of Zn-MnO$_2$ batteries.

Anode **Thickness (μm)**	**Cathode** **Mass loading (mg cm^{-2})**	**Electrolyte**	**Current density (A g^{-1})**	**Cycle number**	**Cumulative capacity (mAh cm^{-2})**
This work **Cu^{2+}-Zn@Cu$_{0.7}$Zn$_{0.3}$** **30**	**Zn$_x$MnO$_2$** **5.5**	**2 M ZnSO$_4$ + 0.2 M MnSO$_4$**	**0.246**	**800**	**847**
Zn@ZSO[6] **100**	K$_{0.27}$MnO$_2$ **8**	2 M ZnSO$_4$ + 0.1 M MnSO$_4$	0.308	400	548
Zn[7] **10**	MnO$_2$ **5.76**	2 M ZnSO$_4$ + 2 mM SeO$_2$	0.2	60	84
Zn[8] **10**	MnO$_2$-**4.5**	2 M ZnSO$_4$ + DFA	0.5	150	67.5
	MnO$_2$-**1.5**			1000	260
Zn[9] -	NCMO-**1**	2 M ZnSO$_4$ + 0.1 M MnSO$_4$	0.5	100	41
	NCMO-**7.5**		0.1	100	140
	NCMO-**10.9**		0.1	50	112.5
Zn[10] -	Al$_{0.1}$MnO$_2$ **1.5**	2 M ZnSO$_4$ + 0.1 M MnSO$_4$	0.2	200	94
Zn[11] -	KMO/Ti$_3$C$_2$ **1.1**	2 M ZnSO$_4$ + 0.1 M MnSO$_4$+0.4 M K$_2$SO$_4$	0.3	125	46.2
MPVMT@Zn[12] **80**	MnO$_2$ **1**	2 M ZnSO$_4$ + 0.1 M MnSO$_4$	0.616	500	80
Zn@ZBO[13] **20**	MnO$_2$ **20**	2 M ZnSO$_4$ + 0.1 M MnSO$_4$	0.154	100	406
(C$_2$F$_4$)$_n$-C@Cu@Zn[14] **24**	CNT/MnO$_2$ **1.3**	2 M ZnSO$_4$ + 0.1 M MnSO$_4$	0.2	200	39
PDMS/TiO$_2$-x@Zn[15] -	α-MnO$_2$ **1.5**	3 M ZnSO$_4$	0.308	400	107.2
FPCH-ZI/Zn[16] **100**	α-MnO$_2$@CNT **1**	2 M ZnSO$_4$ + 0.1 M MnSO$_4$	0.5	600	132
10	α-MnO$_2$@CNT **2.6**			1000	390
P(VDF-TrFE)@Zn[17] **50**	α-MnO$_2$ **1**	2 M ZnSO$_4$ + 0.1 M MnSO$_4$	0.2	300	48
ZnTe@Zn[18] **10**	MnO$_2$-**3.97**	2 M ZnSO$_4$ + 0.1 M MnSO$_4$	0.616	500	245
	MnO$_2$-**6.33**			500	285

References

1. Q. Chen, J. Jin, Z. Kou, C. Liao, Z. Liu, L. Zhou, J. Wang and L. Mai, *Small*, 2020, **16**, 2000091.
2. J. Hafner, *J. Comput. Chem.*, 2008, **29**, 2044−2078.
3. J. Perdew, K. Burke and M. Ernzerhof, *Phys. Rev. Lett.*, 1996, **77**, 3865.
4. M. Ernzerhof and G. Scuseria, *J. Chem. Phys.*, 1999, **110**, 5029−5036.
5. S. Grimme, J. Antony, S. Ehrlich and H. Krieg, *J. Chem. Phys.*, 2010, **132**, 154104.
6. R. Guo, X. Liu, F. Xia, Y. Jiang, H. Zhang, M. Huang, C. Niu, J. Wu, Y. Zhao and X. Wang, *Adv. Mater.*, 2022, **34**, 2202188.
7. C. Huang, X. Zhao, Y. Hao, Y. Yang, Y. Qian, G. Chang, Y. Zhang, Q. Tang, A. Hu and X. Chen, *Adv. Funct. Mater.*, 2022, **32**, 2112091.
8. H. Tian, J. Yang, Y. Deng, W. Tang, R. Liu, C. Xu, P. Han and H. Fan, *Adv. Energy Mater.*, 2023, **13**, 2202603.
9. X. Gao, C. Shen, H. Dong, Y. Dai, P. Jiang, I. Parkin, H. Zhang, C. Carmalt and G. He, *Energy Environ. Sci.*, 2024, **17**, 2287–2297.
10. Y. Zhao, S. Zhang, Y. Zhang, J. Liang, L. Ren, H. J. Fan, W. Liu and X. Sun, *Energy Environ. Sci.*, 2024, **17**, 1279–1290.
11. H. Qiao, X. Zhu, X. Li, Y. Wang, C. Ye, L. Ma, J. Shen and M. Ye, *Adv. Energy Mater.*, 2024, **14**, 2304357.
12. Z. Zheng, X. Zhong, Q. Zhang, M. Zhang, L. Dai, X. Xiao, J. Xu, M. Jiao, B. Wang and H. Li, *Nat. Commun.*, 2024, **15**, 753.
13. D. Wang, H. Liu, D. Lv, C. Wang, J. Yang and Y. Qian, *Adv. Mater.*, 2023, **35**, 2207908.
14. Q. Li, H. Wang, H. Yu, M. Fu, W. Liu, Q. Zhao, S. Huang, L. Zhou, W. Wei and X. Ji, *Adv. Funct. Mater.*, 2023, **33**, 2303466.
15. Z. Guo, L. Fan, C. Zhao, A. Chen, N. Liu, Y. Zhang and N. Zhang, *Adv. Mater.*, 2022, **34**, 2105133.
16. J. Park, C. Choi, J. Park, S. Yu and D. Kim, *Adv. Energy Mater.*, 2022, **12**, 2202937.
17. Y. Wang, T. Guo, J. Yin, Z. Tian, Y. Ma, Z. Liu, Y. Zhu and H. Alshareef, *Adv. Mater.*, 2022, **34**, 2106937.
18. R. Wang, S. Xin, D. Chao, Z. Liu, J. Wan, P. Xiong, Q. Luo, K. Hua, J. Hao and C. Zhang, *Adv. Funct. Mater.*, 2022, **32**, 2207751.